Learning of Cluster-based Feature Importance for Electronic Health Record Time-series

Henrique Aguiar [1] **Mauro Santos** [1] **Peter Watkinson** [2] **Tingting Zhu** [1]

Abstract

The recent availability of Electronic Health Records (EHR) has allowed for the development of algorithms predicting inpatient risk of deterioration and trajectory evolution. However, prediction of disease progression with EHR is challenging since these data are sparse, heterogeneous, multi-dimensional, and multi-modal time-series. As such, clustering is regularly used to identify similar groups within the patient cohort to improve prediction. Current models have shown some success in obtaining cluster representations of patient trajectories. However, they i) fail to obtain clinical interpretability for each cluster, and ii) struggle to learn meaningful cluster numbers in the context of imbalanced distribution of disease outcomes. We propose a supervised deep learning model to cluster EHR data based on the identification of clinically understandable phenotypes with regard to both outcome prediction and patient trajectory. We introduce novel loss functions to address the problems of class imbalance and cluster collapse, and furthermore propose a feature-time attention mechanism to identify cluster-based phenotype importance across time and feature dimensions. We tested our model in two datasets corresponding to distinct medical settings. Our model yielded added interpretability to cluster formation and outperformed benchmarks by at least 4% in relevant metrics.

1. Introduction

A variety of medical settings are characterised by the existence of multiple distinct patient subgroups, largely distinguished by differences in pathology, response to treatment and medical interventions, etc. Identifying and characterising such subgroups is key to better understand underlying disease(s) and improve the delivery of medical care. For instance, the management of highly impactful chronic diseases such as Chronic Obstructive Pulmonary Disease (COPD) and Cardiovascular Disease (CVD), (Adeloye et al., 2015), has improved with the identification of subgroups with different exacerbation profiles, (Turner et al., 2015; Vogelmeier et al., 2018).

Electronic Health Records (EHR) time-series data are typically used to determine clinically relevant subgroups, and have been applied, e.g., to detect the risk of deterioration. However, modelling disease progression and risk prediction is challenging due to the extreme data heterogeneity nature of EHRs. Firstly, EHR data contains a mixture of demographic or static variables (such as age and sex), and multi-dimensional time-series (e.g Heart Rate, HR, and laboratory measurements, such as blood tests). Secondly, EHR time-series are multi-modal as different features are collected from different devices, representing distinct clinical properties of relevance. Similarly, time-series features are sampled at different times and have low and distinct sampling rates, as well as different missing value properties. Furthermore, each feature is associated with different noise and evolution patterns.

Recent advances in deep learning (DL) approaches have shown promising results in EHR modelling due to their capacity to handle complex data (Rajkomar et al., 2018). Nonetheless, DL approaches typically lack relevant interpretability frameworks which are key to scaling and deploying such tools in hospital settings. Several models have since been proposed to tackle this issue (Mayhew et al., 2018), however, most of them focus on a subset of EHR features (usually vital signs only), consider one-dimensional input data and fail to provide a clinically-focused phenotypic analysis of learnt patient subgroups (via clustering).

This work builds on previous research by introducing a cluster-based feature-time attention mechanism to improve the prediction of patient outcomes through EHR data. Our method also leverages phenotypic information to aid in clinical interpretability, not only making use of demographic and vital-sign information, but also of relevant laboratory measurements (all present in the EHR) to provide a more complete patient physiological status. Our contributions

[1]Department of Engineering Science, University of Oxford, United Kingdom [2]Nuffield Department of Clinical Neurosciences, University of Oxford, United Kingdom. Correspondence to: Henrique Aguiar <henrique.aguiar@eng.ox.ac.uk>.

Proceedings of the 39^{th} International Conference on Machine Learning, Baltimore, Maryland, USA, PMLR 162, 2022.

include the following:

- An end-to-end DL supervised model to cluster EHR patient data based on the identification of clinically meaningful cluster phenotypes with regard to both outcome prediction and patient trajectory in a multi-class setting;
- A weighted loss to address target outcome imbalance for both tasks of clustering and prediction, a common issue in the medical domain;
- The incorporation of a novel loss mechanism to address the issue of cluster collapse and promote sample assignment to all available clusters;
- Finally, the inclusion of a novel interpretability framework, derived from a cluster-based feature-time attention layer, which aims to identify relevant timestamps and feature variables pairs to represent the patient physiology, cluster assignment and, ultimately, outcome prediction.

This paper is structured as follows. In Section 2, we describe previous research in EHR time-series modelling, clustering and attention methods. Section 3 introduces both datasets we used in our analysis, while section 4 describes our proposed model. The experimental setup and results of our analysis are consequently presented in Section 5 and discussion takes place in Section 6. Finally, concluding remarks and ideas for future work are available in Section 7.

2. Related Work

EHR data comprise complex time-series data, being high-dimensional, multi-modal and heterogeneous, and thus presenting challenges when used in machine learning models (Keogh & Kasetty, 2003; Rani & Sikka, 2012). An important goal in a medical setting is to identify phenotypically separable clusters with distinct phenotypic profiles (which we denote as phenotypic clustering hereafter). For the purposes of this work, cluster phenotypes result from the combination of two distinct components: a) the evolution of patient feature trajectories' within the cluster, and b) the characterisation of the cluster with regard to clinical variables of interest. The latter may include features not used for clustering and may provide information about the underlying or future health status.

Traditional clustering models such as K-Means or hierarchical clustering have been shown to fail to capture the existing time-dependent feature relationships when modelling EHR. As such, variants have been proposed to mitigate this problem. A temporal version of the K-Means algorithm, Time-Series K-Means (TSKM, Tavenard et al. (2020)), considers different distances in time-series space, including a temporal Euclidean distance (which is equivalent to considering all feature temporal observations as an independent feature value for the corresponding patient admission), and other alignment strategies such as Dynamic-Time Warping (DTW, Berndt & Clifford (1994)) and a differentiable approximation, soft-DTW (Cuturi & Blondel, 2017).

Recent DL architectures, ranging from Auto-Encoders (AE, Ma et al. (2019)), Convolutional Neural Networks (CNN, Munir et al. (2019)) and others, have shown great promise when applied to time-series data across a variety of domains. Fortuin et al. (2019) proposed a Self-Organising Map - Variational Auto-Encoder (SOM-VAE) model, which represents a state-of-the-art, unsupervised, DL clustering algorithm. SOM-VAE extends a variational auto-encoder architecture (Kingma & Welling, 2014) to represent observations through the addition of a Markov model (Gagniuc, 2017) to infer temporal evolution within the latent space. Clustering is performed in the low dimensional embeddings with a SOM (Kohonen, 1982) to obtain a discrete, topologically-interpretable latent representation of the learnt clusters. Alternatively, through the usage of supervised outcome labels, AC-TPC (Lee & Schaar, 2020) serves as the current state-of-the-art for identifying phenotypically separable clusters in patient trajectories in EHR data. AC-TPC maps EHR data into a latent space via an encoder, and uses an actor-critic framework (Konda & Tsitsiklis, 2003) which leverages clinical outcomes to aid in cluster formation. Neither SOM-VAE and AC-TPC provide clinically meaningful interpretation of feature-time importance, i.e. at what time and what feature is driving cluster assignment, or outcome of interest.

Attention mechanisms have recently been proposed to provide greater interpretability to Recurrent Neural Networks (RNN) and to aid in dealing with long-term dependencies (Vaswani et al., 2017; Xu et al., 2015). They have also been used in modelling EHR time-series (Schwab et al., 2017; Shashikumar et al., 2018). RETAIN (Choi et al., 2016) proposes a two-level reverse attention mechanism to mimic a physician's decision process and predict a future diagnosis. In other recent works, attention mechanisms based on bi-directional RNN and CNN outperformed standard classification models in predicting high risk vascular diseases with the addition of medication information as input data (Kim et al., 2017). A drawback of such attention mechanisms is the focus on temporal interpretability only, and the inability to look at individual features, which is key in a medical setting. To solve this issue, (Shamout et al., 2020) considered independent RNN per feature, with a concatenation of the resulting latent vectors. However, the latter does not allow the joint modelling across both feature and time dimensions. Alternatively, (Kaji et al., 2019; Gandin et al., 2021) proposed learning attention weights directly on the original inputs, prior to being transformed by a RNN, which

does not allow modelling of the resulting latent representations. To the best of our knowledge, no existing models have been proposed that jointly leverage both feature and time dimensions (feature-time) to determine clinical observation relevance for clustering EHR data.

3. Dataset and Pre-Processing

To validate the usefulness of our model, we consider 2 distinct medical datasets, corresponding to different environments within the healthcare system. We first discuss a proprietary, secondary care dataset in section 3.1 which was the main motivation behind our modelling innovations. Afterwards, in order to be able to provide further validation of our methods, as well as assess their reproducibility, we present a freely-available dataset of an emergency ward environment in section 3.2, which also provides support to our claims of generalisability of our model to other healthcare settings.

3.1. HAVEN

We first consider HAVEN, a dataset retrieved from a retrospective database of routinely collected observations from concluded hospital admissions between March 2014 and March 2018 (HAVEN project, REC reference: 16/SC/0264 and Confidential Advisory Group reference 08/02/1394). The database includes EHR measurements of adult patients admitted to four hospitals from the Oxford University Hospitals NHS Foundation Trust. Note that the HAVEN dataset does not include data from Intensive Care Units (ICU), and we have excluded observations taken in the Emergency Department (ED). Key characteristics of HAVEN cohort data include a) heterogeneity, b) multi-modality, and difference in: c) noise distributions, d) sampling rates, e) missing values. Such properties are common across EHR settings, and are challenging with respect to learning useful representations and predictions.

We used the protocol defined in (Pimentel et al., 2019) to subset the cohort to those patients at risk of developing Type-II Respiratory Failure (T2RF) in hospital (a diagram of the data selection steps can be found in Figure A.1 in the Appendix). Four patient outcomes were considered in our analysis: i) no event during the hospital stay, leading to successful discharge from the hospital, or the first instance of one of three possible events, ii) unplanned entry to ICU, iii) cardiac arrest (also named 'Cardiac' hereafter) and iv) 'Death'. Outcome groups data features are not clearly separable (see Tables A.2, A.3 in the Appendix), so patient clusters will naturally contain a mix of different admission outcomes. In this setting, the clinically relevant component of a cluster phenotype (henceforth denoted as *cluster outcome propensity* or *cluster propensity*) is represented as a categorical distribution indicating the corresponding likelihood for cluster-assigned patients to have the corresponding outcome. This can be the empirical outcome proportion distribution over a cluster, but can also be any other categorical distribution learnt by models.

For each admission, observational data were averaged into 4 hour-window blocks, based on the time to outcome (or time to discharge, in the case of no event during stay). Following the literature validating Early Warning Score (EWS) systems (baseline models used by UK NHS staff to track inpatient physiology, (RCP, 2017)) and clinical input, only observations within 24 and 72 hours before the outcome were considered, such that the target phenotype represents the patient status in the subsequent 24 hours. Features were transformed according to min-max normalization due to skewness and heterogeneity in their distributions. Patient admissions were randomly split into train, validation and test sets. Missing values were imputed based on the previously observed time block - all remaining missing observations were imputed according to the feature median from the aggregated validation and test data (see Section 5 for the description of train-test data split). Imputed values were flagged in a three-dimensional mask matrix.

After processing, input data contained over 100,000 patient trajectories corresponding to 4,266 unique hospital admissions (only the last admission of each patient was considered in our analysis). Original trajectories for the patient cohort are shown in the Appendix in Figures A.4, A.5, A.6 for different variables/features. A lack of clear outcome group separability can be observed across temporal and static variables. Furthermore, we note the high degree of imbalance in the data - admissions with no event account for over 86.8% of the total number of admissions, while event classes correspond to 10.3% Death, 1.8% ICU and 1.1% Cardiac.

3.2. MIMIC-IV ED

In order to test the validity of our model in a different setting, as well as improve the reproducibility of our work, we also considered a dataset representing admissions to an emergency department, MIMIC-IV-ED (Johnson et al., 2021; Goldberger et al., 2000), abbreviated simply as MIMIC. MIMIC is a large, freely available database of ED admissions at the Beth Israel Deaconess Medical Center between 2011 and 2019, containing 448,972 ED admissions ('stays'). For each admission, MIMIC contains information on vital-sign data, triage information, medications and hospital journey.

We followed a similar pre-processing method as to HAVEN. We disregarded admissions related to psychiatry and/or childbirth as these represent significantly distinct cohorts of the general population. We applied temporal aggregation into 1 hour blocks, and we considered only observations at most 6 hours before ED discharge time. We decided

on these values based on data distribution and clinical input. We defined four outcomes for each patient admission based on their journey throughout the following 12 hours: a) whether the patient died ('Death'), b) whether the patient was admitted to ICU ('ICU'), c) whether the patient remained at a hospital ward ('Discharge'), and d) whether the patient was discharged ('Ward'). After processing, the event classes were distributed as 0.30% Death, 16.53% ICU, 2.11% Discharge and 81.06% Ward, which shows the high level of imbalance in this dataset.

4. Methods

4.1. Proposed model

We propose a novel model, which we denote by **C**luster-b**A**sed i**M**portanc**E** **L**earning f**O**r **T**ime-series (CAMELOT). Our proposed methodology is displayed in Figure 1[1]. Our model improves on previous literature on 3 key items: a) a modified loss function to target the multi-class imbalance, b) a novel loss function to ensure cluster exploration and representative clustering, and c) a novel feature-time attention-level framework to boost representation and introduce feature-time interpretability for cluster assignment.

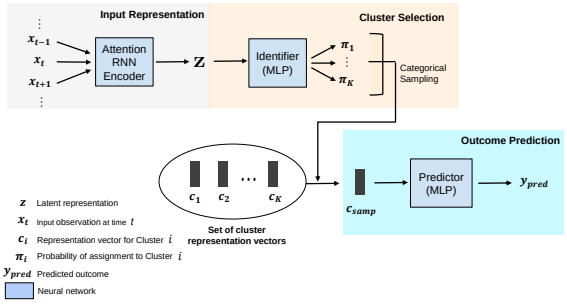

Figure 1. Diagram of proposed model. MLP - Multilayer Perceptron neural network blocks; RNN - Recurrent Neural Network.

Let N denote the number of patients and D_f the number of input features. Input data consists of a set of patient trajectories $\mathbb{X} = \{\{\mathbf{x}_{n,t}\}_{t=1}^{T_n}\}_{n=1}^{N}$, where T_n is the maximum number of temporal observations for patient n, and a set of patient outcomes $\mathbb{Y} = \{\mathbf{y}_n\}_{n=1}^{N}$. Input trajectory data for the n-th patient is represented as $\mathbf{X}_n = [\mathbf{x}_{n,1}, ..., \mathbf{x}_{n,T_n}]$, where each $\mathbf{x}_{n,t} \in \mathbb{R}^{D_f}$ is referred to as an *observation* (vector), with a maximum of observed D_f feature values. The corresponding patient outcome is a *one-hot encoded* vector $\mathbf{y}_n \in \mathbb{R}^4$ (more generally, the dimension of $\mathbf{y}_n$ equals to the number of possible outcomes).

Our DL model can be decomposed into 3 neural network blocks: an Encoder, Identifier and Predictor. We refer the action of each network respectively as E, I and P (for example, $I(\mathbf{x})$ denotes the output of the Identifier given some input vector $\mathbf{x}$). Both the Identifier and Predictor are Multilayer Perceptrons (MLP), networks of stacked feed-forward dense layers. On the other hand, the Encoder block can be further sub-divided into a) a stack of RNN layers and b) our proposed custom attention layer (see Section 4.2 for further details). Separately, we also consider a set of *trainable* cluster representation vectors, $\mathcal{C} = \{\mathbf{c}_1, ..., \mathbf{c}_K\}$. We assign the outcome for cluster i as $P(\boldsymbol{c}_i)$.

A model call is as follows: Given the n-th patient input trajectory data $\mathbf{X}_n$, the Encoder network returns a *latent representation* $\mathbf{z}_n := E(\mathbf{X}_n) \in \mathbb{R}^l$. Consequently, the Identifier network computes cluster assignment probabilities, $\boldsymbol{\pi}_n := I(\mathbf{z}_n) \in \mathbb{R}^K$. Each element of $\boldsymbol{\pi}_n$, π_n^i, represents the probability assignment of $\mathbf{z}_n$ to cluster i, given a total of K clusters. A cluster, k_{samp}^n is selected according to categorical sampling ($k_{\text{samp}}^n \sim \text{Cat}(\boldsymbol{\pi}_n)$), and the corresponding cluster representation, $\mathbf{c}_{\text{samp}}^{\mathbf{n}} := \mathbf{c}_{\mathbf{k}_{\text{samp}}^{\mathbf{n}}}$ is then selected from $\mathcal{C}$. The output of the model is $y_{\text{pred}} := P(\mathbf{c}_{\text{samp}}^n) \in \mathbb{R}^4$. We note that k_{samp}^n is only sampled during a *training phase*; at prediction stage, cluster selection follows the equation $k_{\text{pred}}^n = \underset{i=1,...,K}{\arg\max}\, \pi_n^i$.

4.2. Encoder Network and a Custom Attention Layer

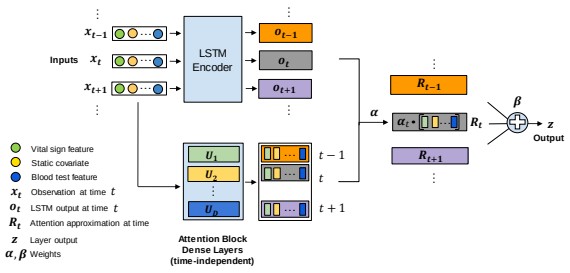

Figure 2. Diagram of the Encoder network composed of an LSTM Encoder and a custom attention layer.

The diagram of our proposed Encoder network is presented in Figure 2. The Encoder contains (i) a Recurrent Neural Network (RNN) block of stacked Long Short-Term Memory (LSTM) layers, and (ii) a customised attention layer, which computes a latent representation by comparing input data with the sequence of output states from the RNN block. We use the same notation as above, and write the sequence of output states of the final LSTM layer as $\mathbf{o}_{n,1}, ..., \mathbf{o}_{n,T_n}$, with $\mathbf{o}_{n,i} \in \mathbb{R}^l$. Theoretically, each $\mathbf{o}_{n,t}$ corresponds to a representative summary of input patient information up until time t. We propose to approximate $\mathbf{o}_{n,t}$ as a linear

[1]Code for our model can be found on the github repository CAMELOT-ICML

combination of latent representations of each individual feature, thereby allowing the separation of output states into contributions from each feature. Note that it is important for the feature transformations to be *time-independent* in order to avoid over-parametrising and over-fitting the model, and to ensure feature representation maps are similar across time.

Our attention layer behaves as a set of D_f feed-forward neural network layers, $\mathbf{U}_1, ..., \mathbf{U}_{D_f}$, jointly represented by: (i) a matrix of *learnable* kernel weights $\boldsymbol{D} \in \mathbb{R}_{l \times D_f}$. We write $\boldsymbol{D} = [\mathbf{D}_1, ..., \mathbf{D}_{D_f}]$; (ii) a matrix of *learnable* bias vectors $\boldsymbol{B} \in \mathbb{R}_{l \times D_f}$. Similarly, we can write $\boldsymbol{B} = [\mathbf{B}_1, ..., \mathbf{B}_{D_f}]$; and (iii) an activation function, σ which matches the output activation of the RNN block.

Input data for patient n, $\mathbf{X}_n$ is fed as input to the RNN block, which outputs a sequence of latent output states $(\mathbf{o}_{n,t})_{t=1}^{T_n}$. For $t = 1, ..., T_n$, we compute D_f feature representations in latent space as:

$$\boldsymbol{R}_{n,t} := \sigma(\boldsymbol{D} \odot \mathbf{x}_{n,t} + \boldsymbol{B}) \tag{1}$$

where $\boldsymbol{R}_{n,t} = [\mathbf{R}_{n,t}^1, ..., \mathbf{R}_{n,t}^{D_f}]$ is our collection of feature representations, σ is applied element-wise and $\mathbf{A} := \boldsymbol{D} \odot \mathbf{x}_{n,t}$ is a matrix satisfying $A_{i,j} = \boldsymbol{D}_{i,j}(\mathbf{x}_{n,t})_j$. Equivalently, $\mathbf{R}_{n,t}^i$ is the output of a dense layer, $\mathbf{U}_i$ with kernel $\mathbf{D}_i$, bias $\mathbf{B}_i$, activation σ and input $(\mathbf{x_{n,t}})_i$. We approximate $\mathbf{o}_{n,t} \approx \sum_{i=1}^{D_f} \alpha_t^i \mathbf{R}_{n,t}^i = \boldsymbol{R}_{n,t}\boldsymbol{\alpha}_t$. This approximation is minimised following a least squares criterion, which has a well-known solution, $\widehat{\boldsymbol{\alpha}}_t$, and corresponding optimal approximation $\widehat{\mathbf{o}}_{n,t} = \boldsymbol{R}_{n,t}\widehat{\boldsymbol{\alpha}}_t$.

Given, $\hat{\mathbf{o}}_{n,t}$, we compute a context vector as $\mathbf{z} := \sum_t \beta_t \hat{\mathbf{o}}_{n,t}$, where weights $\boldsymbol{\beta}$ are learned to provide a more representative context vector. This is the latent representation of patient n and output of the Encoder network.

4.3. Attention Map Visualisation

Given cluster representation vectors, $\mathbf{c}_k$, we can compute a cluster-wise feature-time attention visualisation map as follows. First, we normalise feature-weights $\widehat{\boldsymbol{\alpha}}_t$ according to a softmax function, $\mathbf{s}_t = \sigma(\widehat{\boldsymbol{\alpha}}_t) \in \mathbb{R}^{D_f}$, where σ is the softmax function: $\sigma(\mathbf{x}) = \frac{\exp|\mathbf{x}|}{\|\exp|\mathbf{x}|\|_1}$. Note we take the absolute value inside the softmax function - consequently, we extract importance from the magnitude of linear approximation weights, as opposed to simply prefering the largest values.

Secondly, we compute cluster-wise weights, γ_t^k according to a temporal least-square approximation of $\mathbf{c}_k \approx \sum_{t=1}^{T_n} \widehat{\mathbf{o}}_{n,t}\gamma_{n,t}^k$, and solved as before. We similarly normalise $\gamma_{n,t}^k$ to obtain cluster temporal scores, $e_{n,t}^k = \sigma(\gamma_{n,t}^k)$. Finally, we can compute K scoring matrices, $M_n^1, ..., M_n^K \in \mathbb{R}_{T_n \times D_f}$: $\left(M_n^k\right)_{t,f} = e_{n,t}^k \boldsymbol{s}_t^f$. Note that: $\|M_n^k\|_1 = \sum_t e_{n,t}^k \sum_f \boldsymbol{s}_t^f = \sum_t e_{n,t}^k = 1$. Given that matrices M_n^k are normalised we visualise them as a normalised feature-time map for cluster assignment relevance, which we use to provide further model interpretability.

4.4. Loss optimisation

The model is optimised through consideration of three distinct loss functions. We introduce a weighted cross-entropy loss function:

$$L_{\text{pred}}(y_{\text{true}}, y_{\text{pred}}) = -\sum_{c=1}^{C} w_c y_{\text{true}}^c \log\left(y_{\text{pred}}^c\right)$$

This loss is equivalent to $L = -w_{c'} \log(y_{\text{pred}})_{c'}$, where c' is the true outcome for a particular patient. We propose inversely proportional normalised weights: $\sum_{c=1}^{C} w_c = 1$ and w_c is inversely proportional to the class distribution, i.e., $w_c \propto \frac{N}{N_c}$ with N being the number of patients and N_c being the number of patients with outcome label c. Class weighting penalises misclassification more heavily on less sampled classes.

We also propose a novel distribution loss function, $L_{\text{dist}}(\boldsymbol{\pi})$. Define the average cluster probability of assignment as $\boldsymbol{\pi}_C := \frac{1}{N}\sum_n \boldsymbol{\pi}_n$. Then we introduce $L_{\text{dist}}(\boldsymbol{\pi}) = -H(\boldsymbol{\pi}_C)$, where H denotes information entropy. Note that L_{dist} is minimised when π_C is uniform, ensuring all clusters are 'explored' and have comparable number of samples. Finally, to separate cluster representation vectors, we define the cluster separation loss as $L_{\text{clus}}(\mathcal{C}) = -\frac{1}{K(K-1)}\sum_{i,j} \|\mathbf{c}_i - \mathbf{c}_j\|^2$.

Both L_{dist} and L_{clus} are important to address an issue we call *cluster collapse*, a phenomenon observed during training where clusters may tend to collapse. This can result from either i) sample assignment to a small subset of clusters (thus not exploring further phenotypes) and ii) convergence of learnt cluster embeddings (so that cluster representations are largely indistinguishable).

To optimise our model, iterative gradients are applied according to weighted combinations of the above loss functions with hyper-parameter weights α, β:

1. Firstly, the Predictor is updated according to L_{pred};
2. After, the Encoder and Identifier are trained according to $L_{\text{pred}} + \alpha L_{\text{dist}}$;
3. Finally, cluster representation vectors are updated with regards to $L_{\text{pred}} + \beta L_{\text{clus}}$.

4.5. Initialisation

Our proposed model also follows a set of initialisation pretraining procedures. Firstly, the Encoder and Outcome

Predictor are pre-trained according to a classification task ($\tilde{\mathbf{y}} = P(E(\mathbf{x}))$), with corresponding loss L_{pred}. Latent state representations $E(\mathbf{x})$ are clustered through a K-means algorithm with K clusters across the whole training set. Cluster representation vectors are initialised as given by the resulting cluster centroids, and finally the Cluster Identifier network is pre-trained to identify clusters as predicted by the K-Means algorithm with categorical cross-entropy loss. We also tested our models with other non-K-means clustering initialisation of embeddings, but did not observe a significant difference in results.

Model implementation was completed in Python, with TensorFlow 2, scikit-learn and NumPy. All experiments were run with 1 Tesla v100 GPU, and 8 CPUs Intel(R) Xeon(R) Gold 6246 @ 3.30GHz.

5. Results

5.1. Setup

In order to compare our models against other approaches, we consider a set of clustering benchmarks. We compare with TSKM as a classic clustering method (with Euclidean, DTW and soft-DTW distances considered), and SOM-VAE and AC-TPC as state-of-the-art phenotypic clustering methods. AC-TPC receives as input temporal subsequences of a complete patient set of observations - for comparison purposes, we consider only the model output for the complete patient sequence. For simplicity, we present results with all input features considered, except where indicated otherwise.

All models were trained on the same training set (60% of the complete input data) and evaluated against the same test set (remaining 40%). For DL models, we further split the training set into a purely training and validation sets. All sets considered contain data corresponding to distinct patients. All experiments with varying hyper-parameters were repeated 10 times with a fixed set of 10 distinct seeds, and results are reported according to average metric performance and standard deviation. A complete list of the hyper-parameters considered for each model is included in Table A7 in the Appendix. In bold, top-performing hyper-parameters are indicated. Optimal integer hyper-parameters (K, l) were selected according to an "Occam's Razor" approach - for each parameter, we assign it the highest value such that increasing this amount does not lead to a significant increase in performance according to the mean AUROC and a Friedman's hypothesis test. Neural network size parameters were kept consistent across all DL models where applicable. All other optimal hyper-parameters were selected according to the highest AUROC performance conditional on the model predicting at least a sample for each class (e.g. not simply separating, say, non-Death and Death classes).

We evaluated clustering performance through standard clustering metrics, including Silhouette score (SIL, (Rousseeuw, 1987)), Davies-Bouldin Index (DBI, (Davies & Bouldin, 1979)), Variance Ratio Criterion (VRI, (Calinski & Harabasz, 1974)). Results on HAVEN for all clustering models are displayed in Table 3, with a similar trend observed in MIMIC. We also consider the predictive ability of our clustering framework. In Tables 5 and 4 , we evaluated the (multi-class) prediction performance with regards to Area-under-the-Receiver-Operating-Curve (AUROC), unweighted mean F1-score, unweighted mean Recall, and Normalised Mutual Information (NMI). For purely unsupervised models (SOM-VAE and TSKM), an outcome predictive pipeline was constructed by assigning patient admissions to clusters, and consequently to the empirical outcome distribution in the corresponding cluster.

Metric	TSKM	SOM-VAE	AC-TPC	CAMELOT
SIL	**0.35 (±0.01)**	0.25 (± 0.08)	0.04 (± 0.01)	0.11 (±0.04)
DBI	**1.19 (±0.08)**	1.89 (± 0.63)	4.34 (± 0.80)	3.12 (±0.53)
VRI	**554.6 (±2.50)**	12.8 (± 9.32)	66.5 (± 18.7)	216.7 (±6.2)

Table 3. Clustering separability results on HAVEN dataset by the different clustering methodologies given input data with all available features (static, vital-signs, serum and haematological variables). For each metric and model, the average score and standard deviation are returned. The best values for each metric are indicated in bold.

Metric	AUROC	F1-score	Recall	NMI
SVM	0.68 (± 0.00)	0.25 (± 0.00)	0.27 (± 0.00)	0.05 (± 0.00)
XGB	**0.73 (±0.01)**	0.29 (± 0.00)	0.28 (± 0.00)	0.08 (± 0.001)
TSKM	0.64 (± 0.03)	0.22 (± 0.00)	0.20 (± 0.00)	0.00 (± 0.00)
SOM-VAE	0.62 (± 0.03)	0.21 (±0.01)	0.20 (± 0.00)	0.02 (± 0.00)
AC-TPC	0.58 (± 0.02)	0.23 (±0.01)	0.25 (± 0.01)	0.02 (± 0.00)
CAMELOT	0.72 (±0.02)	**0.34 (±0.02)**	**0.36 (±0.02)**	**0.11 (±0.03)**

Table 4. Outcome prediction scores across all models on MIMIC dataset, displayed with an average and standard deviation of a set of 10 seeds. Note that NEWS2 is not applicable on the MIMIC Emergency Department setting. The best values for each metric are indicated in bold. For clustering algorithms, cluster outcome distributions were taken to be the empirically observed distribution in each cluster.

Metric	AUROC	F1-score	Recall	NMI
SVM	0.59 (± 0.02)	0.23 (± 0.00)	0.25 (± 0.00)	0.01 (± 0.02)
XGB	0.65 (± 0.01)	0.23 (± 0.00)	0.22 (± 0.00)	0.03 (± 0.04)
NEWS2	0.61	0.29	0.34	0.01
TSKM	0.55 (± 0.01)	0.24 (± 0.03)	0.26 (± 0.02)	0.01 (± 0.03)
SOM-VAE	0.61 (± 0.09)	0.27 (± 0.05)	0.27 (± 0.03)	0.05 (± 0.03)
AC-TPC	0.68 (± 0.01)	**0.38 (±0.01)**	0.36 (± 0.01)	0.17 (± 0.02)
CAMELOT	**0.73 (±0.02)**	0.36 (±0.01)	**0.38 (±0.02)**	**0.20 (±0.03)**

Table 5. Outcome prediction scores across all models on HAVEN dataset, displayed with an average and standard deviation of a set of 10 seeds (except NEWS2, which is deterministic). The best values for each metric are indicated in bold. For clustering algorithms, cluster outcome distributions were taken to be the empirically observed distribution in each cluster.

This prediction task was also benchmarked against other classifiers for outcome prediction in EHR data, namely Sup-

port Vector Machines (SVM), XGBoost (XGB) and NEWS2 (i.e., the National Early Warning Score used in the UK hospitals). Given that these algorithms are naturally derived from tabular data, we consider slight modifications to apply them to time-series data in order to act as faithful predictive benchmarks. NEWS2 considers only a fixed set of observations - as such, for each patient we output the score of the latest input observation. For SVM and XGB, we consider 2 alternative solutions to build a temporal classifier. The first approach concatenates temporal time-series into a large, single feature vector of size $T_n \times D_f$, which is then passed as input. Separately, we also considered an ensemble model where SVM/XGB were independently trained on univariate time-series data (i.e. for a single feature), and consequently aggregated to obtain a predictive score for the multi-dimensional temporal input. This is so that temporal variation can be modelled by the benchmarks for a fair comparison. Finally, note that the complete NEWS Score is not applicable on the MIMIC Emergency Department setting.

5.2. Ablation Studies

We also conducted ablation studies on our proposed model on the predictive task. We use the following notation: a) CAMELOT denotes the original model; b) ABL1 (or ATTEP), where we replace the proposed L_{dist}, with sample-wise entropy loss proposed in AC-TPC; c) ABL2 (or ENC-PRED), which removes the clustering component of CAMELOT, leaving only the Encoder and Predictor. To evaluate the relevance of our loss functions and attention layer, we also consider d) ABL3 as CAMELOT with $\alpha = 0$ (i.e. no L_{dist}), e) ABL4 as CAMELOT with $\beta = 0$ (no L_{clus}), f) ABL5 as CAMELOT with $\alpha = \beta = 0$ and g) ABL6 as CAMELOT without the attention layer. Ablation results are presented in Tables 6 (HAVEN) and 7 (MIMIC).

Metric	AUROC	F1-score	Recall	NMI
ABL1	0.67 (± 0.02)	0.36 (±0.02)	0.36 (± 0.02)	0.16 (± 0.03)
ABL2	0.57 (± 0.02)	0.25 (±0.02)	0.26 (± 0.02)	0.06 (± 0.03)
ABL3	0.65 (± 0.01)	0.30 (±0.02)	0.32 (± 0.02)	0.15 (± 0.01)
ABL4	0.65 (± 0.02)	0.28 (±0.01)	0.30 (± 0.00)	0.15 (± 0.01)
ABL5	0.61 (± 0.04)	0.25 (±0.02)	0.27 (± 0.01)	0.10 (± 0.03)
ABL6	0.69 (± 0.01)	0.36 (±0.01)	0.36 (± 0.01)	0.18 (± 0.01)
CAMELOT	**0.73 (±0.02)**	**0.36 (±0.01)**	**0.38 (±0.02)**	**0.20 (±0.03)**

Table 6. Outcome prediction scores on HAVEN across ablation models. Results report mean and standard deviation over a fixed set of 5 seeds.

Metric	AUROC	F1-score	Recall	NMI
ABL1	0.69 (± 0.01)	0.25 (±0.01)	0.33 (± 0.02)	0.07 (± 0.01)
ABL2	0.65 (± 0.03)	0.23 (±0.01)	0.26 (± 0.01)	0.04 (± 0.00)
ABL3	0.70 (± 0.01)	0.30 (±0.01)	0.34 (± 0.00)	0.07 (± 0.00)
ABL4	0.70 (± 0.02)	0.24 (±0.03)	0.31 (± 0.04)	0.05 (± 0.02)
ABL5	0.67 (± 0.03)	0.30 (±0.01)	0.33 (± 0.01)	0.06 (± 0.00)
ABL6	0.65 (± 0.05)	0.24 (±0.01)	0.30 (± 0.02)	0.04 (± 0.01)
CAMELOT	**0.72 (±0.02)**	**0.34 (±0.02)**	**0.36 (±0.02)**	**0.11 (±0.03)**

Table 7. Outcome prediction scores on MIMIC across ablation models. Results report mean and standard deviation over a fixed set of 5 seeds.

5.3. Phenotyping and Characterisation

On top of performance evaluation with regards to clustering separability and outcome prediction, we display the learnt phenotypes by our proposed model in comparison with the learnt cluster phenotypes of the phenotypic clustering benchmark AC-TPC. For each cluster, the corresponding outcome propensity $P(\mathbf{c})$ is shown as a bar plot over the 4 possible outcomes with a corresponding probability value. For completeness, we also display cluster outcome propensity plots for both TSKM and SOM-VAE in the Appendix (Figures A.8 and A.9). Note that the cluster outcome propensity distributions learnt by CAMELOT (learnt as part of model training and without any computation involving the patients' true outcome) also align with the empirical outcome relevance in the learnt clusters (Table A.12). Lastly, we also display feature-time cluster relevance attention maps in Figure 9. For a given cluster $j \in \{1, ..., K\}$, we consider all patients assigned to cluster j, denoted by C_j, and compute the average attention matrix for the cluster $M^j = \frac{1}{|C|_k} \sum_{\text{pat}_n \in C_j} M_n^j$ (refer also to Section 4.3). We then display it as a normalised heatmap across clusters. For simplicity and due to the motivation of this work, we display these results on the HAVEN dataset for vital-signs and static variables, but this work can naturally be extended to different temporal sets of features.

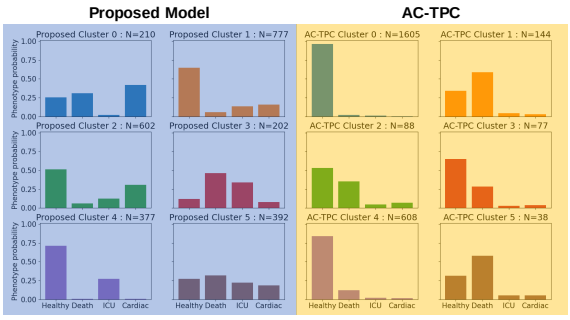

Figure 8. Comparison of bar plots of cluster outcome propensity distributions for the proposed model and benchmark AC-TPC. On the left (blue), distributions are displayed for each cluster (out of a total of 6), and each phenotype corresponds to the probability of an outcome. Similar results are shown on the right (yellow) for AC-TPC. The title of each sub-plot indicates the cluster considered, as well as the number of patients assigned to a given cluster. Cluster sizes are also indicated. It can be observed that AC-TPC learnt phenotypes are less diverse than those learnt by our proposed model.

6. Discussion

Our proposed model shows an improvement in clustering performance (see Table 3) when compared to the current phenotypic clustering benchmark (AC-TPC), and outper-

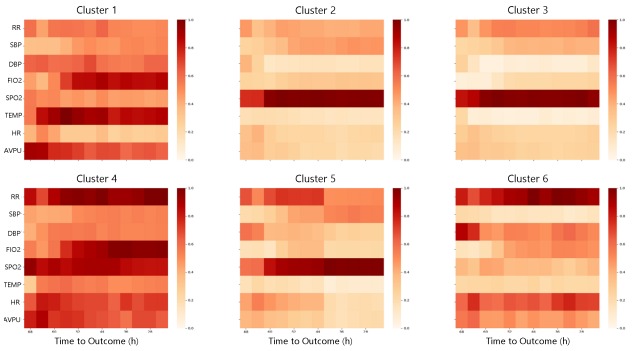

Figure 9. Average attention feature maps for each cluster on HAVEN dataset. Given cluster c, we compute the average cluster attention matrix for patients in this cluster. Maps are represented as a normalised heatmap across all clusters. The horizontal axis represents the time to outcome, in hours, while the vertical axis indicates vital-sign feature.

forms SOM-VAE according to VRI. Although the cluster separability metrics are superior in the case of TSKM, this is expected given a metric bias towards convex clusters, and the convexity resulting from TSKM being a K-Means based algorithm. Furthermore, DL clustering occurs in a latent space, which, unfortunately, is not easily comparable with an algorithm targeting the input space (such as K-Means). We argue clusters learnt by TSKM are less relevant than those learnt from our model. Using HAVEN results as an example, TSKM clusters are extremely hard to distinguish with regards to outcome propensity (as evidenced by very low performance on a prediction task (see Tables 4 and 5)). Furthermore, TSKM clusters are less separable with regard to trajectory evolution, as there is less separation of mean HR trajectories, and less cluster separation when data are projected to a two-dimensional domain with t-stochastic neighbour embedding (tSNE) (see Figures A10 and A11 in the Appendix).

Concerning predictive power, which was used to select hyper-parameters as the most important task, our model performed much better than all benchmarks with two exceptions (where competitive performance is attained). On the HAVEN dataset, it can be seen in Tables 4 and 5 that our model outperforms both standard classifiers (at least 8%) and benchmarking clustering methods (at least 5%) according to mean AUROC. A similar increase can be seen in other classification metrics, with the exception of F1-score, where model performance is slightly below (but very comparable) to that of AC-TPC. On the other hand, on MIMIC we outperform all models by 4% on mean AUROC, with the exception of XGB (which has a similar confidence interval compared to CAMELOT). However, we are significantly better (5% in F1-score, 8% in Recall and 3% in NMI) than other methods over the other scores. Given that other metrics are more class-sensitive than average AUROC, our model is better at identifying smaller sample-sized classes than other models, which was observed empirically as XGB and SVM could not identify the two smaller sampled classes.

Our model is able to more accurately determine patterns in the data than the previously proposed models, as EHR data is extremely complex and heterogeneous. It is particularly promising that the model obtains good predictive task results despite a clustering bottleneck (i.e. predicted outcomes for a given patient are done through the assigned cluster, as opposed to tailored to the precise input data). While it is possible that other models could show better performance on the direct task of outcome prediction given EHR input, such models can potentially be associated with a lack of robustness or input sensitivity difficulties. Furthermore, it is likely they would struggle with identifying relevant trends and properties of clinical interest. As such, for new admissions, these models could provide a prediction for the overall outcome, but no robust understanding of how this outcome will occur, and how to prevent potential risks of deterioration, let alone the ability to pool data from other similar patients.

Figure 8 shows the advantage of two key aspects of our methodology (we show results on the HAVEN dataset for simplicity). Our model identifies clear, separable cluster outcome distributions and provides a useful layer of interpretability for clinicians to understand a potential risk of deterioration. CAMELOT also identifies a more diverse set of cluster outcomes than AC-TPC, which only picks up 3 different cluster outcome distributions, and doesn't identify the presence of the "ICU" and "Cardiac" classes. With regards to clusters learnt by CAMELOT, clusters 0 and 3 are the clusters with the most ill cohort - they are largely representative of death and cardiac events on the subsequent 24 hours. On the other hand, clusters $2, 5$ are healthier, with a smaller chance of adverse events. Clusters 1 and 4 are largely "healthy" clusters, with reduced risks of the most intense adverse events. We note cluster outcome propensity distributions learnt by AC-TPC are unable to provide this level of detailed information. Furthermore, the propensity distribution learnt by our model largely matches the empirical number of outcome events observed in each cluster (displayed in Appendix Table A12). Moreover, the model managed to successfully resolve a heavy class-imbalance setting and identify the much smaller classes. Representative clusters are able to capture different-sized sub-populations, yet still identify potential risks of deterioration. We also show other cluster-phenotype benchmark results in Appendix A.8 and A.9., and it can be seen the phenotypes identified here are not as clinically meaningful.

Learnt cluster attention maps shown in Figure 9 introduce yet another layer of interpretability to our proposed cluster-

ing model. The average attention maps highlight the relevant feature-time pairs driving patient cluster assignment, and can be used to identify the most important clinical variables. For instance, analysis of Figure 8 suggests clusters with the highest propensity for either Death or Cardiac Arrest events are Clusters 0, 3 (and 2 to a slightly smaller extent). This reflects in the resulting attention maps, where RR, FIO_2 and SpO_2 are highlighted as key clinical variables for cluster assignment. This conclusion is further corroborated when considering descriptive statistics of CAMELOT clusters (Table A14), as the three are some of the few variables with some significant separation across clusters, and also considering trajectory evolution (Figure A13). Lastly, note that feature-time weights are also relevant if potential deterioration events did not take place - so that we are more confident about a patient's health status. As an example, attention maps for clusters 1 and 4 (reasonably healthy clusters) indicate SpO_2 as very relevant throughout the admission - this is likely due to these patients not showing a worsening of blood oxygenation. Thus, the learnt attention maps can be very versatile.

7. Conclusion and Future Work

In this work, we propose a novel deep learning model for the task of identification of phenotypically separable clusters applied to EHR data. As part of our model, we consider 2 loss functions over previous SOTA and introduce a novel feature-time attention layer to better represent patient data and to introduce a feature-time relevance map for each cluster. Our experiments show promising results with the addition of both methodological tools above, on both cluster separability and outcome prediction performance. The addition of the feature-time layer has the added benefit of introducing key interpretability tools for researchers to understand relevant regions for good patient physiology representation as well as an indication of what can lead to patient deterioration.

There are multiple interesting avenues of investigation building on this work. On the one hand, the current attention layer mechanisms could potentially be improved with the addition of temporal weight smoothness, or, alternatively, weight regularization to encourage smooth exploration of the complete feature-time space. Similarly, this layer could be extended to work well with missing data to ensure that temporal features that were sampled at different rates capture the attention of the model differently. The observed issue of cluster collapse warrants further exploration, both in terms of the development of theoretical frameworks for this phenomenon, but also with regard to introducing statistical guarantees to address it. Furthermore, our methodological improvements will also benefit from more extensive testing across other diverse imbalanced datasets and other potential areas of application.

Acknowledgements

Thank you to all the reviewers for their valuable feedback and input. For their work in data curation and preparation, we would like to thank Dr. Marco Pimentel and Dr. Oliver Redfern. We would also like to extend our thanks to Dr. David Prytech and Dr. Gary Smith for their clinical input in understanding our methodologies. HA is supported by the EPSRC Center for Doctoral Training in Health Data Science (EP/S02428X/1). MS was funded/supported by the National Institute for Health Research (NIHR) Biomedical Research Centre (BRC), Oxford. PW was supported by the NIHR Biomedical Research Centre, Oxford. TZ was supported by the Engineering for Development Research Fellowship provided by the Royal Academy of Engineering. This publication was supported by the Health Innovation Challenge Fund (HICF-R9-524; WT103703/Z/14/Z), a parallel funding partnership between the Department of Health and Wellcome Trust. The views expressed are those of the author(s) and not necessarily those of the NHS, the NIHR or the Department of Health.

References

Adeloye, D., Chua, S., Lee, C., Basquill, C., Papana, A., Theodoratou, E., Nair, H., Gasevic, D., Sridhar, D., Campbell, H., Chan, K. Y., Sheikh, A., and Rudan, I. Global and Regional Estimates of COPD Prevalence: Systematic Review and Meta-analysis. *Journal of Global Health*, 5, 2015.

Berndt, D. J. and Clifford, J. Using Dynamic Time Warping to Find Patterns in Time Series. *Proceedings of the 3rd International Conference on Knowledge Discovery and Data Mining*, pp. 359–370, 1994.

Calinski, T. and Harabasz, J. A Dendrite Method for Cluster Analysis. *Communications in Statistics*, 3:1–27, 1974.

Choi, E., Bahadori, M., Kulas, J., Schuetz, A., Stewart, W., Sun, J., and Health, S. RETAIN: An Interpretable Predictive Model for Healthcare using Reverse Time Attention Mechanism. *Proceedings of the 30th International Conference on Neural Information Processing Systems*, pp. 3512–3520, 2016.

Cuturi, M. and Blondel, M. Soft-DTW: a Differentiable Loss Function for Time-Series. *Proceedings of the 34th International Conference on Machine Learning - Volume 70*, pp. 894–903, 2017.

Davies, D. L. and Bouldin, D. W. A Cluster Separation Measure. *IEEE Transactions on Pattern Analysis and Machine Intelligence*, PAMI-1:224–227, 2 1979.

Fortuin, V., Hüser, M., Locatello, F., Strathmann, H., and Rätsch, G. SOM-VAE: Interpretable Discrete Repre-

sentation Learning on Time Series. *Proceedings of the International Conference on Learning Representations 2019*, 6 2019.

Gagniuc, P. A. *Markov Chains: From Theory to Implementation and Experimentation*. John Wiley & Sons, 1st edition, 6 2017.

Gandin, I., Scagnetto, A., Romani, S., and Barbati, G. Interpretability of Time-Series Deep Learning Models: A Study in Cardiovascular Patients Admitted to Intensive Care Unit. *Journal of Biomedical Informatics*, 121, 9 2021.

Goldberger, A. L., Amaral, L. A., Glass, L., Hausdorff, J. M., Ivanov, P. C., Mark, R. G., Mietus, J. E., Moody, G. B., Peng, C. K., and Stanley, H. E. PhysioBank, PhysioToolkit, and PhysioNet: Components of a New Research Resource for Complex Physiologic Signals. *Circulation*, 101:215–220, 6 2000.

Johnson, A., Bulgarelli, L., Pollard, T., Celi, L. A., Mark, R., and Horng, S. MIMIC-IV-ED (version 1.0). *PhysioNet*, 2021.

Kaji, D. A., Zech, J. R., Kim, J. S., Cho, S. K., Dangayach, N. S., Costa, A. B., and Oermann, E. K. An Attention based Deep Learning Model of Clinical Events in the Intensive Care Unit. *PloS one*, 14, 2 2019.

Keogh, E. and Kasetty, S. On the Need for Time Series Data Mining Benchmarks: A Survey and Empirical Demonstration. *Data Mining and Knowledge Discovery*, 7:349–371, 10 2003.

Kim, Y. J., Lee, Y.-G., Kim, J. W., Park, J. J., Ryu, B., and Ha, J.-W. Highrisk Prediction from Electronic Medical Records via Deep Attention Networks. *Proceedings of the 31st Conference on Neural Information Processing Systems*, 11 2017.

Kingma, D. P. and Welling, M. Auto-Encoding Variational Bayes. *Proceedings to the International Conference on Learning Representations (ICLR) 2014*, 2014.

Kohonen, T. Self-Organized Formation of Topologically Correct Feature Maps. *Biological Cybernetics 1982 43:1*, 43:59–69, 1 1982.

Konda, V. R. and Tsitsiklis, J. N. On Actor-Critic Algorithms. *SIAM Journal on Control and Optimization*, 42: 1143–1166, 8 2003.

Lee, C. and Schaar, M. V. D. Temporal Phenotyping using Deep Predictive Clustering of Disease Progression. *Proceedings of the 37th International Conference on Machine learning*, pp. 5767–5777, 6 2020.

Ma, Q., Zheng, J., Li, S., and Cottrell, G. W. Learning Representations for Time Series Clustering. *Proceedings of the 33rd Conference of Neural Information Processing Systems (NeurIPS 2019)*, 12 2019.

Mayhew, M. B., Petersen, B. K., Sales, A. P., Greene, J. D., Liu, V. X., and Wasson, T. S. Flexible, Cluster-based Analysis of the Electronic Medical Record of Sepsis with Composite Mixture Models. *Journal of Biomedical Informatics*, 78:33–42, 2 2018.

Munir, M., Siddiqui, S. A., Dengel, A., and Ahmed, S. DeepAnT: A Deep Learning Approach for Unsupervised Anomaly Detection in Time Series. *IEEE Access*, 7:1991–2005, 1 2019.

Pimentel, M. A., Redfern, O. C., Gerry, S., Collins, G. S., Malycha, J., Prytherch, D., Schmidt, P. E., Smith, G. B., and Watkinson, P. J. A Comparison of the Ability of the National Early Warning Score and the National Early Warning Score 2 to Identify Patients at Risk of in-Hospital Mortality: A Multi-Centre Database Study. *Resuscitation*, 134:147–156, 1 2019.

Rajkomar, A., Oren, E., Chen, K., Dai, A. M., Hajaj, N., Hardt, M., Liu, P. J., Liu, X., Marcus, J., Sun, M., Sundberg, P., Yee, H., Zhang, K., Zhang, Y., Flores, G., Duggan, G. E., Irvine, J., Le, Q., Litsch, K., Mossin, A., Tansuwan, J., Wang, D., Wexler, J., Wilson, J., Ludwig, D., Volchenboum, S. L., Chou, K., Pearson, M., Madabushi, S., Shah, N. H., Butte, A. J., Howell, M. D., Cui, C., Corrado, G. S., and Dean, J. Scalable and Accurate Deep Learning with Electronic Health Records. *npj Digital Medicine*, 1:18, 5 2018.

Rani, S. and Sikka, G. Recent Techniques of Clustering of Time Series Data: A Survey. *International Journal of Computer Applications*, 52:1–9, 8 2012.

RCP. National Early Warning Score (NEWS) 2 Standardising the Assessment of Acute-Illness Severity in the NHS - Updated Report of a Working Party. *Clinical medicine (London, England)*, 19, 2017.

Rousseeuw, P. Silhouettes: A Graphical Aid to the Interpretation and Validation of Cluster Analysis. *Journal of Computational and Applied Mathematics*, 20:53–65, 11 1987.

Schwab, P., Scebba, G. C., Zhang, J., Delai, M., and Karlen, W. Beat by beat: Classifying cardiac Arrhythmias with Recurrent Neural Networks. *Computing in Cardiology*, 44, 2017.

Shamout, F. E., Zhu, T., Sharma, P., Watkinson, P. J., and Clifton, D. A. Deep Interpretable Early Warning System for the Detection of Clinical Deterioration. *IEEE Journal*

Appendix

Data

A description of the complete pipeline of data pre-processing, following the protocol defined in (Pimentel et al., 2019), is shown in Figure A.1.

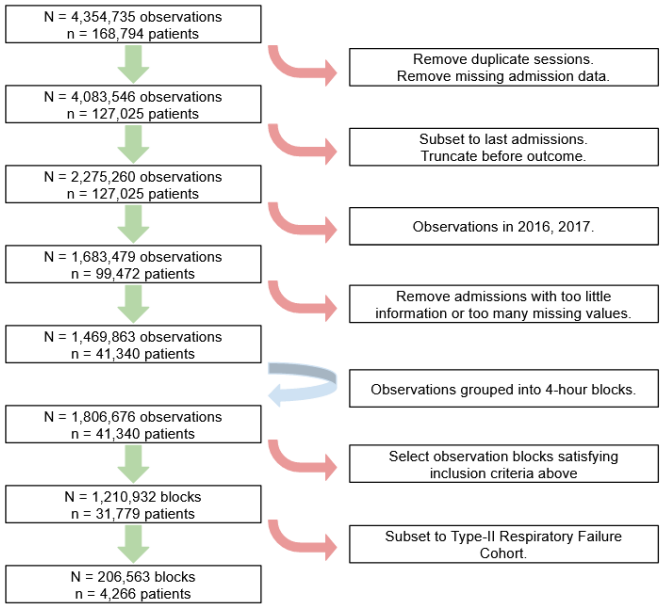

A.1. HAVEN data pre-processing steps.

A total of 26 input features were considered. Firstly, 4-hourly vital-sign sets which included 8 features: Heart Rate (HR), Respiratory Rate (RR), Systolic Blood Pressure (SBP), Diastolic Blood Pressure (DBP), peripheral Oxygen Saturation (SpO_2), Temperature (TEMP), level of consciousness via the AVPU scale - Alert, Verbal, Pain, Unresponsive - and estimated Fraction of Inspired Oxygen (FiO_2, available when an oxygen mask is applied to the patient). Each set consisted of a timestamp and the vital-sign numerical values. Secondly, 4 demographic variables were selected (modelled as static variables): age, sex, and admission type (elective or surgical). Thirdly, we included 6 features resulting from biochemistry blood tests, denoted as 'Serum': Serum levels of urea, albumin, creatinine, sodium, potassium and C-reactive protein concentrations. Finally, 8 haematological blood test features were also included: white and haemaglobin cell counts, concentration of eosinophils, basophils, neutrophils, and lymphocytes, as well as eosinophil-to-basophil and neutrophil-to-lymphocyte ratios. These features were selected based on domain knowledge of features related to severity in the prognosis and outcome of inpatients at risk of T2RF.

Descriptive statistics for all input variables is described in Table A.2. Median and inter-quartile range (IQR) is displayed for continuous and categorical variables, while binary variables are shown according to number of counts in the dataset and corresponding cohort proportion. Statistics are displayed for the complete data ("All"), but also for each sub-cohort defined by the overall outcome. We can observe that these sub-cohorts are not clearly separable and are hard to identify solely from this information.

A summary of the patient cohort in relation to outcomes and target phenotypes can be seen in Table A.3. Challenges with regards to obtaining phenotypically separable clusters can similarly be observed - there is no clear significant difference between the target outcome sub-cohorts with regards to demographic input variables. With regards to outcome distribution, we also note the high degree of imbalance in the dataset - the large majority of the patients in our dataset suffered from no adverse events (over 86%), while only 48 had a Cardiac event, and 76 were re-directed to the ICU.

The lack of outcome sub-cohort separability can be further observed in a temporal domain. Figures A.4, A.5, A.6 plot

	Description	Units	Type	All	Cardiac	ICU	Death	Healthy
n	Patient Count		Integer	4266	48	76	441	3701
N	Trajectory Count		Integer	110,916	1,248	1,976	11,466	96,226
O	Observation Count		Integer	1,206,119	14,095	20,227	184, 504	1,067,293
Vital signs								
HR	Heart-rate	beats/minute (bpm)		82.50 (72 - 94)	88 (77 - 100)	88.50 (77 - 99)	89 (77 - 100)	81.67 (72 - 92)
RR	Respiratory-Rate	breaths/minute (Bpm)		18 (16 - 19)	18.29 (17.50 - 20)	18 (16 - 19)	19 (18 - 21)	18 (16 - 18)
SBP	Systolic Blood Pressure	mmHg		126 (112 - 141)	122 (108 - 138)	119 (104 - 137)	123 (108 - 140)	127 (113 - 142)
DBP	Diastolic Blood Pressure	mmHg	Continuous	67 (60 - 76)	65 (57 - 73)	64 (57 - 72.33)	66 (58 - 75)	67 (60 - 76)
SPO2	Estimated Oxygen Saturation	%		95 (94 - 97)	95 (93 - 97)	95 (94 - 97)	94 (91 - 96)	95 (94 - 97)
FIO2	Fraction of Inspired Oxygen concentration	%		21 (21.00 - 28.67)	21 (21 - 31)	21 (21 - 41)	28 (21 - 45)	21 (21 - 21)
TEMP	Temperature	°C		36.40 (36.05 - 36.80)	36.25 (36.00 - 36.60)	36.40 (36.00 - 36.83)	36.20 (36. - 36.65)	36.40 (36.10 - 36.80)
AVPU	Alert, Verbal, Pain, Unresponsive Scale		Categorical (1-4)	1 (1 - 1)	1 (1 - 1)	1 (1 - 1)	1 (1 - 1)	1 (1 - 1)
Static								
age	Patient age	year	Integer	72 (62 - 81)	76 (69 - 82)	69 (61 - 80)	81 (74 - 88)	71 (61 - 74)
gender	Male patients			2123 (49.77 %)	28 (58.33 %)	38 (50.00 %)	247 (56.01 %)	1810 (48.01 %)
Elective	Elective Admissions		Binary	1139 (26.70 %)	2 (4.17 %)	8 (10.53 %)	3 (0.68 %)	1126 (29.42 %)
Surgical	Surgical admissions			1130 (26.49 %)	6 (12.50 %)	22 (28.95 %)	48 (10.88 %)	1054 (28.48 %)
Serum								
HGB	Haemaglobin	g/L		11.20 (9.70 - 12.80)	11.00 (9.35 - 12.40)	10.35 (9.00 - 12.03)	10.80 (9.30 - 12.60)	11.30 (9.80 - 12.90)
WBC	White Blood Cell count (blood)	x10^9/L		10.03 (7.63 - 13.23)	10.90 (8.41 - 15.36)	10.41 (6.79 - 14.04)	11.38 (8.34 - 15.82)	9.80 (7.54 - 12.82)
EOS	EOSinophil count (blood)	x10^9/L		0.10 (0.02 - 0.22)	0.06 (0.01 - 0.20)	0.04 (0.00 - 0.15)	0.03 (0.00 - 0.11)	0.11 (0.03 - 0.24)
BAS	BASophil count (blood)	x10^9/L	Continuous	0.04 (0.02 - 0.05)	0.03 (0.02 - 0.06)	0.03 (0.02 - 0.05)	0.03 (0.02 - 0.05)	0.04 (0.02 - 0.06)
EER	Eosinophil-Basophil Ratio			2.60 (0.75 - 5.50)	1.50 (0.50 - 4.88)	1.48 (0.17 - 4.50)	1.00 (0.00 - 3.33)	3.00 (1.00 - 5.86)
NEU	NEUtrophil count (blood)	x10^9/L		7.60 (5.34 - 10.70)	8.88 (6.25 - 12.60)	8.14 (4.75 - 11.22)	9.31 (6.46 - 13.52)	7.31 (5.19 - 10.19)
LYM	LYMphocyte count (blood)	x10^9/L		1.16 (0.77 - 1.68)	1.00 (0.63 - 1.58)	1.00 (0.55 - 1.62)	0.84 (0.55 - 1.24)	1.24 (0.85 - 1.75)
NLR	Neutrophil-Lymphocyte Ratio			6.36 (3.76 - 11.67)	9.40 (4.88 - 15.98)	8.41 (4.33 - 15.55)	10.84 (6.20 - 19.59)	5.74 (3.31 - 10.11)
Haematological								
ALB	ALBumin level (plasma)	g/L		26.00 (22.00 - 30.00)	23.00 (20.00 - 28.00)	23.00 (19.00 - 27.50)	23.00 (19.00 - 28.00)	27.00 (23.00 - 31.00)
CR	Creatinine level (plasma)	umol/L		77.00 (58.00 - 109.00)	107.00 (78.75 - 154.25)	78.00 (52.00 - 123.75)	93.00 (62.00 - 145.00)	74.00 (58.00 - 102.00)
CRP	C-Reactive Protein level (plasma)	mg/L	Continuous	63.43 (21.30 - 137.58)	51.50 (25.80 - 112.85)	112.20 (32.45 - 226.05)	85.20 (36.20 - 156.35)	58.00 (18.68 - 131.33)
POT	POTassium level (plasma)	mmol/L		4.00 (3.60 - 4.40)	4.20 (3.80 - 4.80)	4.10 (3.70 - 4.50)	4.10 (3.70 - 4.80)	4.00 (3.60 - 4.30)
SOD	SODium level (plasma)	mmol/L		137.00 (134.00 - 140.00)	136.00 (132.00 - 139.00)	136.00 (133.00 - 139.00)	138.00 (134.00 - 142.00)	137.00 (135.00 - 140.00)
UR	URea concentration levels	ml		6.40 (4.40 - 10.40)	10.50 (6.85 - 18.15)	7.05 (4.40 - 11.67)	10.40 (6.40 - 17.50)	5.90 (4.20 - 9.00)

A.2. Descriptive statistics and information of all input data features. Variables are displayed with type, description, units and average statistics. We separate all features according to medical literature, including vital-sign, static, serum and haematological variables, and we also display statistics per outcome sub-cohort, defined as a cohort with those patients assigned to a given outcome.

A.3. Descriptive demographic variable information for each outcome sub-cohort.

	No Event	Death	ICU	Cardiac
N	3701	441	76	48
Age (IQR)	71 (61 - 80)	81 (74 - 88)	69 (61 - 74)	76 (69 - 82)
Gender, M	1810 (48.9%)	247 (56.0%)	38 (50.0%)	28 (58.33%)
CCI (IQR)	4 (3 - 13)	14 (4 - 21)	7 (4 - 17)	15 (4 - 23)
Elective	1126 (30.4%)	3 (0.7%)	8 (10.5%)	2 (4.2%)
Surgical	1054 (28.5%)	48 (10.1%)	22 (29.0%)	6 (12.5%)

the mean trajectories of different temporal variables sets for each outcome sub-cohort, respectively, according to vital signs, haematological and serum features. Mean is calculated based on the time to outcome, and missing observations are disregarded and ignored.

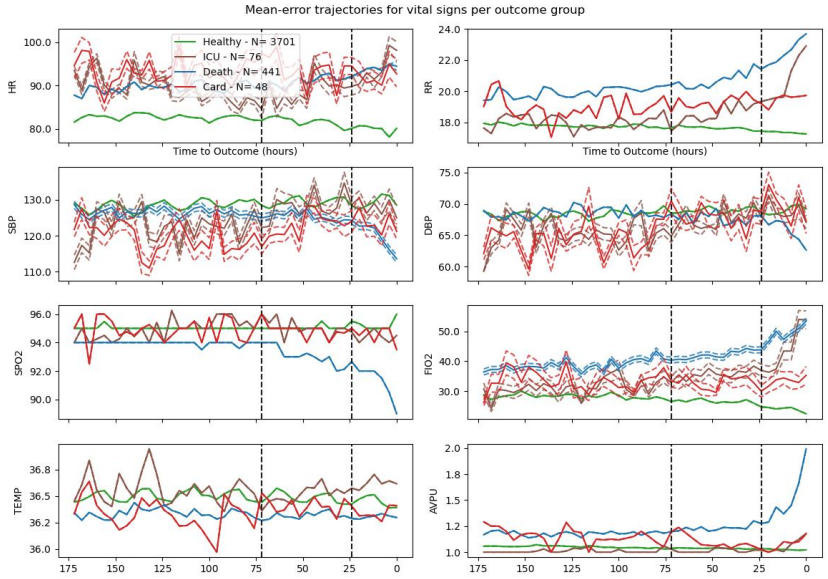

A.4. Plot of mean vital-sign trajectories (median with respect to SpO_2) in solid line as given by the 4 outcome groups: admissions with a) Cardiac-, b) Death- , or c) ICU-, and d) No-events. The corresponding feature units are: HR (bpm), RR (breaths-per-minute), SBP and DBP (mmHg), SPO_2 and FIO_2 (%), TEMP (C) and AVPU is unitless. The respective standard errors are represented by the dashed lines. We visualised trajectories from up to 7 days prior to an outcome event or discharge - the black lines represent the time window (72 - 24 hours prior to an event or discharge) considered for input to all models.

Model Training

A list indicating the grid-search range of hyper-parameters considered in our experiments are indicated in Table A.7. For simplicity, we define $\mathbb{P} := \{0.001, 0.01, 0.1, 1, 10\}$, $\mathbb{L} := \{32, 64, 128, 256\}$ and $\mathbb{K} := \{3, ..., 20\}$. In bold, top-performing hyper-parameters according to target metrics defined in Section 5 are highlighted.

Results Comparison

In Figures A.8 and Figures A.9 we display cluster outcome propensity distributions for some of our experiments with benchmark clustering models SOM-VAE and TSKM, respectively. Both models do not naturally associate clusters with a distribution - we estimate the cluster outcome as the *empirical* outcome distribution for the patient cohort assigned to the corresponding cluster.

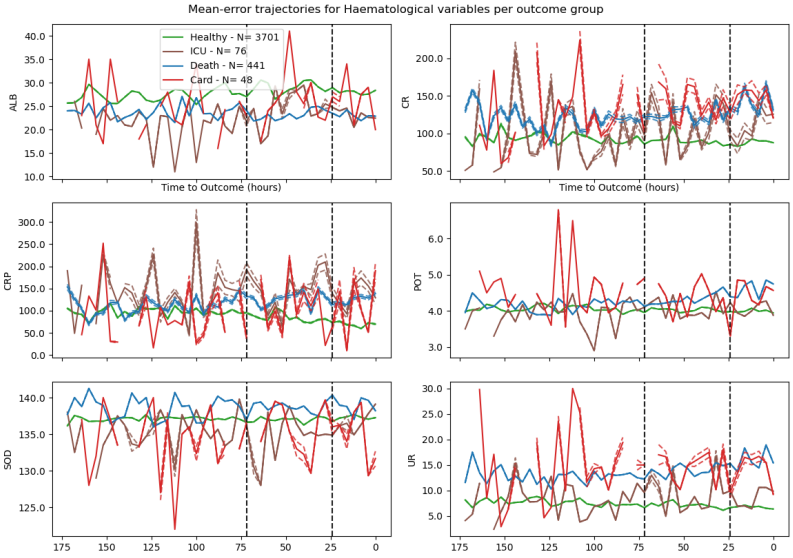

A.5. Plot of mean haematological trajectories in solid line as given by the 4 outcome groups: admissions with a) Cardiac-, b) Death- , or c) ICU-, and d) No-events. The $y-$ axis representations concentration in g/L (ALB), μ mol/L (CR), mmol/L (POT, SOD), mg/L (CRP) and mL (UR). The respective standard errors are represented by the dashed lines. We visualised trajectories from up to 7 days prior to an outcome event or discharge - the black lines represent the time window (72 - 24 hours prior to an event or discharge) considered for input to all models.

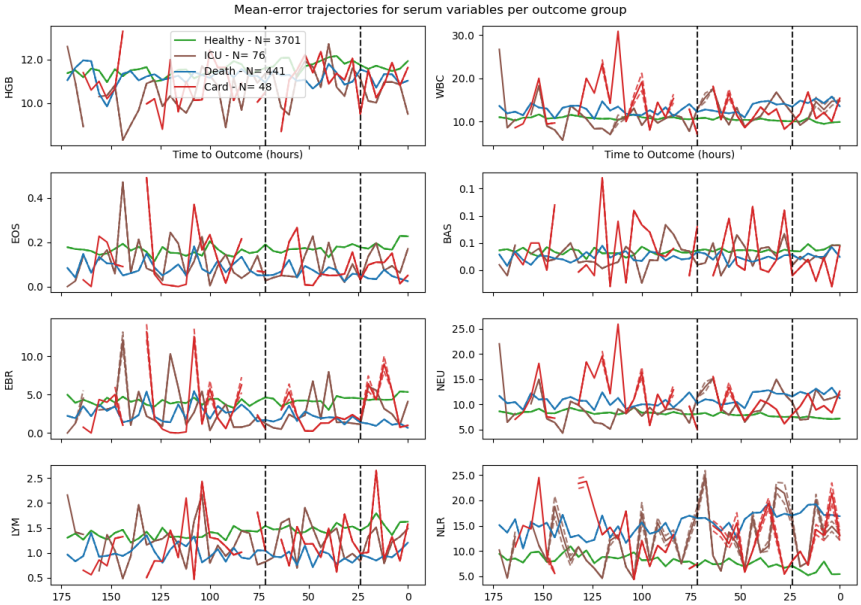

A.6. Plot of mean serum trajectories in solid line as given by the 4 outcome groups: admissions with a) Cardiac-, b) Death- , or c) ICU-, and d) No-events. The $y-$ axis denotes concentration in g/L (HGB) or $10^9/L$ (all other features). The respective standard errors are represented by the dashed lines. We visualised trajectories from up to 7 days prior to an outcome event or discharge - the black lines represent the time window (72 - 24 hours prior to an event or discharge) considered for input to all models.

A.7. Parameter range used for Grid-search hyper-parameter optimisation. For each model, the list of parameter values tested is indicated. In **bold**, the optimum set of hyper-parameters is indicated for each model.

Parameter	TSKM	SOM-VAE	AC-TPC	CAMELOT	SVM	XGB
seeds	$\{1001, 1012, 1134, 2475, 6138, 7415, 1663, 7205, 9253, 1782\}$					
α	-	$\mathbb{P}(\mathbf{0.1})$	$\mathbb{P}(\mathbf{0.01})$	$\mathbb{P}(\mathbf{0.01})$	-	-
β	-	$\mathbb{P}(\mathbf{0.1})$	$\mathbb{P}(\mathbf{0.01})$	$\mathbb{P}(\mathbf{0.001})$	-	-
γ	-	-	-	-	-	$\{0.1, \mathbf{0.2}, 0.6\}$
latent dim	-	$\mathbb{L}(\mathbf{64})$	$\mathbb{L}(\mathbf{128})$	$\mathbb{L}(\mathbf{128})$	-	-
SOM dim	-	$\mathbb{L}^2(\mathbf{4}, \mathbf{4})$	-	-	-	-
K	$\mathbb{K}(\mathbf{7})$	-	$\mathbb{K}(\mathbf{6})$	$\mathbb{K}(\mathbf{6})$	-	-
kernel	{**'DTW'**, 'eucl'}	-	-	-	{**'pol'**, 'rbf'}	-
C	-	-	-	-	$\mathbb{P}(\mathbf{10})$	-
n-estimators	-	-	-	-	-	$\{100, \mathbf{200}, 300\}$
depth	-	-	-	-	-	$\{1, 3, \mathbf{5}, 10\}$
min-child-weight	-	-	-	-	-	$\{1, 2, 3, \mathbf{5}\}$

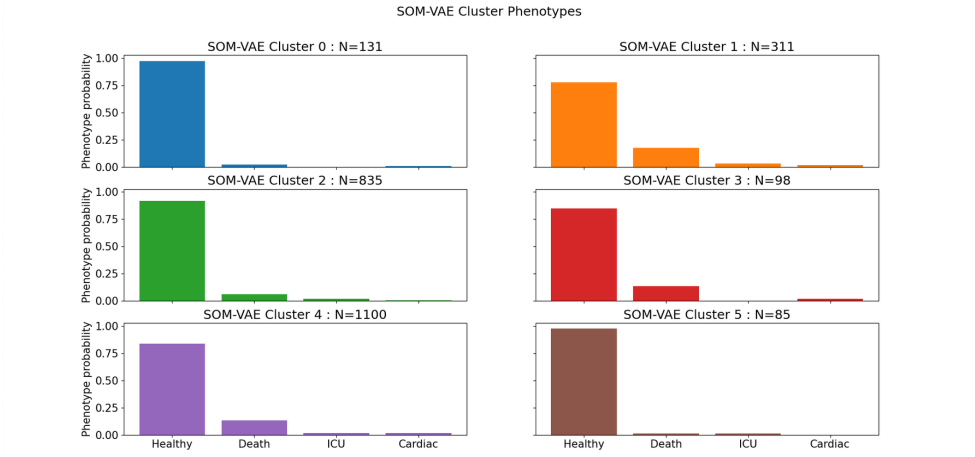

A.8. Bar plots of learnt cluster phenotypes for SOM-VAE with optimal hyper-parameters. Each plot represents a cluster - its phenotype is the corresponding empirical outcome distribution in its cluster-assigned patient cohort.

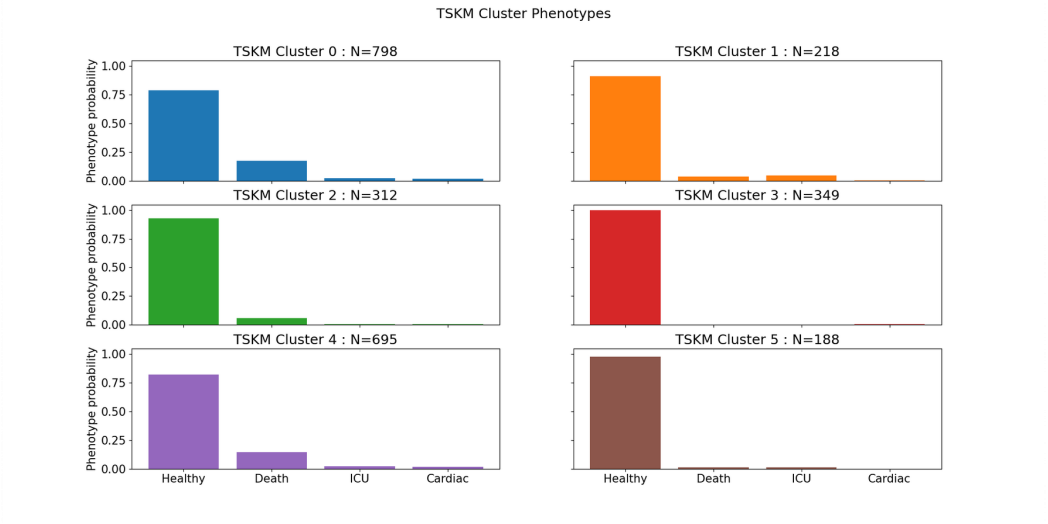

A.9. Bar plots of learnt cluster phenotypes for TSKM with $K = 6$. Each plot represents a cluster - its phenotype is the corresponding empirical outcome distribution in its cluster-assigned patient cohort.

We note that clusters learnt by both clustering benchmark models have identical outcomes, which provides no useful clinical interpretability to the cluster-defined populations, as well as likely not assisting models in learning relevant cluster representations.

We go further in comparing clusters learnt by TSKM and by our proposed model. We argue clusters learnt by CAMELOT are much more relevant towards our goal. We show this through two distinct plots. Firstly, in Figure A10, we display a scatter plot of patients in each cluster (CAMELOT on the right and TSKM clusters on the left) after projection to two dimensions. Projection was completed through a principal component analysis reduction to 50 dimensions, followed by t-stochastic neighbour embedding dimensionality projection to two.

Furthermore, we also demonstrated that TSKM does not learn as separable cluster trajectory evolution profiles as CAMELOT. This is shown in Figure A11, where Heart-Rate mean trajectories for each cluster (i.e., average HR observations aligned to the same time until end of observations for patients in the clusters) are displayed. It is clear that CAMELOT cluster trajectories are easier to separate.

A complete description of the number of patient admissions with a given outcome per learnt cluster in our proposed model can be seen in Table A.12.

A.12. Table with empirical number of outcome admissions observed for each cluster learnt by the proposed model.

Outcome	Healthy	Death	ICU	Cardiac
Cluster 0	149	44	10	7
Cluster 1	739	28	5	5
Cluster 2	579	15	6	2
Cluster 3	93	92	12	5
Cluster 4	373	2	2	0
Cluster 5	288	84	10	10

We also computed summary statistics for the learnt CAMELOT clusters. For each of the resulting clusters, median, and quartile values were computed and plotted, except on the case of binary variables, where only the number of positive

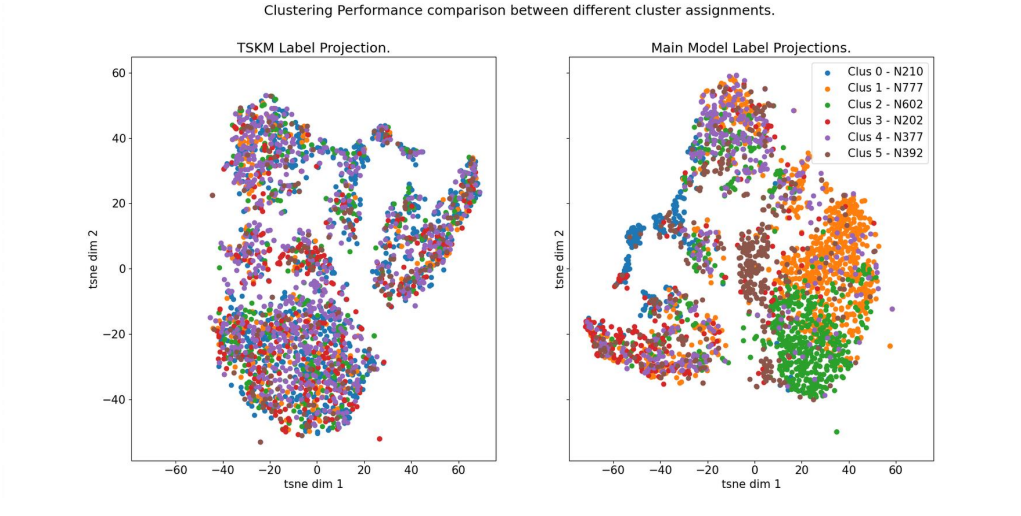

A.10. Scatter plot of cluster patient data after projection to 2 dimensions.

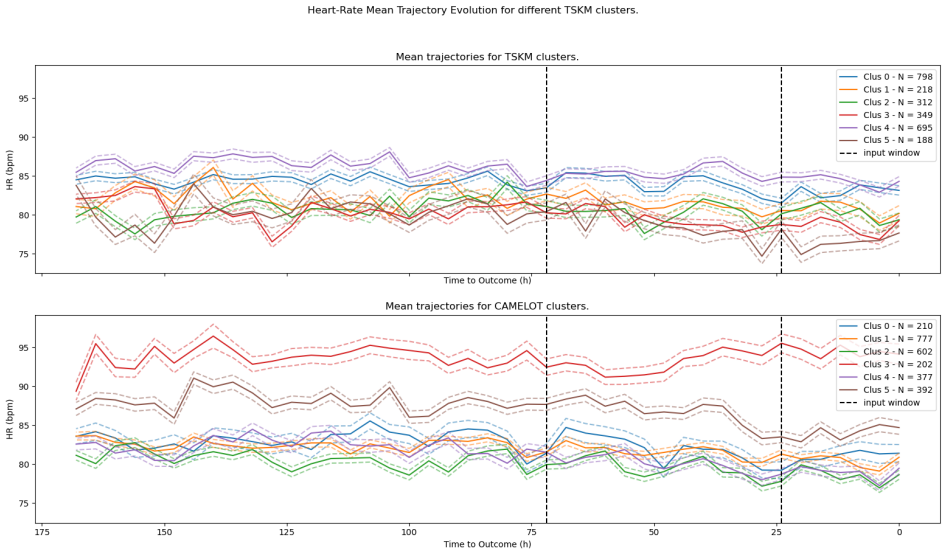

A.11. Plot of mean Heart-Rate (HR) trajectory in solid line as given by the TSKM learnt clusters (top) and CAMELOT (bottom). The respective standard errors are represented by the dashed lines. We visualised trajectories from up to 7 days prior to an outcome event or discharge - the black lines represent the time window (72 - 24 hours prior to an event or discharge) considered for input to all models.

occurrences (and the corresponding proportion in the cluster) are shown. Lastly, we plot the mean cluster trajectory evolution for SBP and FiO_2 to present supportive evidence for the personalised attention maps in Figure 9. These two features were selected from attention map analysis.

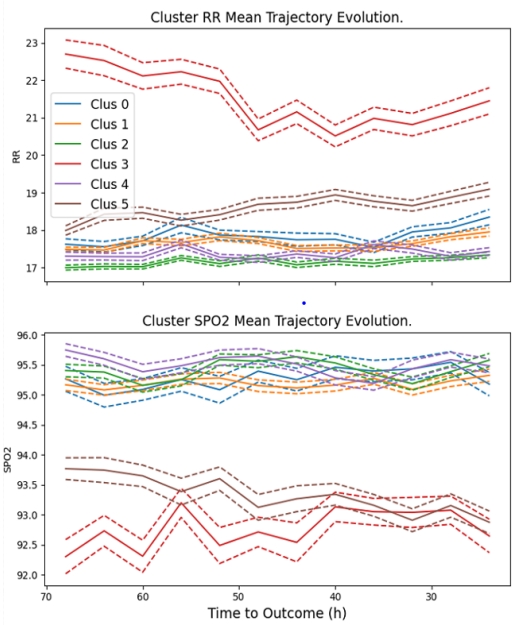

A.13. Plot of mean Respiratory Rate (in breaths-per-minute) trajectories in solid line as given by the clusters learnt by our model (top). In the bottom, mean SPO_2 trajectories (in %) are displayed. The respective standard errors are represented by the dashed lines. We visualised trajectories from up to 7 days prior to an outcome event or discharge - the black lines represent the time window (72 - 24 hours prior to an event or discharge) considered for input to all models.

	n	Description Patient Count	Units	Type Integer	Clus 0 210	Clus 1 777	Clus 2 602	Clus 3 202	Clus 4 377	Clus 5 392
Vital signs										
	HR	Heart-rate	beats/minute (bpm)		82.0 (71.0 - 94.0)	81.0 (72.0 - 91.0)	80.0 (70.4 - 90.0)	93.0 (83.0 - 103.0)	82.0 (72.0 - 92.0)	85.5 (74.0 - 97.0)
	RR	Respiratory-Rate	breaths/minute (Bpm)		18.0 (16.5 - 19.0)	18.0 (16.0 - 18.3)	17.0 (16.0 - 18.0)	19.3 (18.0 - 24.0)	17.0 (16.0 - 18.0)	18.0 (17.0 - 20.0)
	SBP	Systolic Blood Pressure	mmHg		123.0 (107.9 - 142.0)	136.0 (123.0 - 149.0)	117.0 (106.3 - 130.0)	130.0 (115.0 - 143.0)	127.0 (114.0 - 141.0)	123.0 (110.0 - 138.0)
	DBP	Diastolic Blood Pressure	mmHg	Continuous	65.0 (57.0 - 74.0)	70.0 (63.0 - 78.7)	65.0 (58.0 - 72.0)	68.0 (60.0 - 78.0)	67.0 (60.0 - 75.0)	67.0 (59.0 - 75.0)
	SPO2	Estimated Oxygen Saturation	%		95.5 (94.0 - 97.0)	95.0 (94.0 - 97.0)	95.0 (94.0 - 97.0)	94.0 (91.0 - 96.0)	96.0 (94.0 - 97.0)	94.0 (91.0 - 95.5)
	FIO2	Fraction of Inspired Oxygen concentration	%		21.0 (21.0 - 21.0)	21.0 (21.0 - 21.0)	21.0 (21.0 - 21.0)	29.0 (21.0 - 54.0)	21.0 (21.0 - 21.0)	35.0 (21.0 - 49.0)
	TEMP	Temperature	°C		36.3 (36.0 - 36.7)	36.4 (36.1 - 36.8)	36.3 (36.0 - 36.7)	36.4 (36.1 - 36.9)	36.5 (36.2 - 36.9)	36.3 (36.0 - 36.7)
	AVPU	Alert, Verbal, Pain, Unresponsive Scale		Categorical (1-4)	1.0 (1.0 - 1.0)	1.0 (1.0 - 1.0)	1.0 (1.0 - 1.0)	1.0 (1.0 - 1.0)	1.0 (1.0 - 1.0)	1.0 (1.0 - 1.0)
Static										
	age	Patient age	year	Integer	78.0 (69.2 - 84.0)	73.0 (63.0 - 81.0)	71.0 (58.0 - 80.0)	76.5 (69.0 - 85.0)	70.0 (58.0 - 78.0)	72.5 (64.0 - 81.0)
	gender	Male patients			145.0 (69.05 %)	356.0 (45.82 %)	301.0 (50.00 %)	114.0 (56.44 %)	196.0 (51.99 %)	186.0 (47.45 %)
	Elective	Elective Admissions		Binary	30.0 (14.29 %)	210.0 (27.03 %)	178.0 (29.57 %)	8.0 (3.96 %)	124.0 (32.89 %)	110.0 (28.06 %)
	Surgical	Surgical admissions			40.0 (19.05 %)	245.0 (31.53 %)	201.0 (33.39 %)	31.0 (15.35 %)	99.0 (26.26 %)	65.0 (16.58 %)
Serum										
	HGB	Haemaglobin	g/L		9.9 (8.8 - 11.4)	11.4 (10.0 - 13.0)	11.4 (9.7 - 12.9)	11.0 (9.5 - 12.7)	11.1 (9.8 - 12.7)	11.9 (10.4 - 13.2)
	WBC	White Blood Cell count (blood)	x10^9/L		9.9 (7.4 - 13.5)	10.0 (7.8 - 12.9)	9.4 (7.1 - 12.4)	12.5 (8.8 - 17.3)	10.1 (7.8 - 12.9)	10.5 (8.1 - 13.8)
	EOS	EOSinophil count (blood)	x10^9/L		0.1 (0.0 - 0.2)	0.1 (0.0 - 0.2)	0.1 (0.0 - 0.2)	0.0 (0.0 - 0.1)	0.2 (0.1 - 0.4)	0.1 (0.0 - 0.2)
	BAS	BASophil count (blood)	x10^9/L	Continuous	0.0 (0.0 - 0.1)	0.0 (0.0 - 0.1)	0.0 (0.0 - 0.1)	0.0 (0.0 - 0.1)	0.1 (0.0 - 0.1)	0.0 (0.0 - 0.1)
	EBR	Eosinophil-Basophil Ratio			2.8 (0.8 - 5.8)	2.3 (0.8 - 4.6)	2.5 (0.9 - 5.4)	0.8 (0.0 - 3.5)	4.5 (2.3 - 7.6)	2.0 (0.5 - 4.5)
	NEU	NEUtrophil count (blood)	x10^9/L		7.6 (5.5 - 10.8)	7.6 (5.4 - 10.5)	6.9 (4.8 - 9.7)	10.4 (6.6 - 14.6)	7.2 (5.1 - 9.9)	8.2 (6.0 - 11.5)
	LYM	LYMphocyte count (blood)	x10^9/L		0.9 (0.6 - 1.4)	1.2 (0.8 - 1.6)	1.3 (0.9 - 1.8)	0.9 (0.5 - 1.4)	1.4 (1.0 - 2.0)	1.0 (0.7 - 1.5)
	NLR	Neutrophil-Lymphocyte Ratio			8.7 (4.7 - 16.3)	6.4 (3.8 - 10.6)	5.3 (3.2 - 9.1)	12.9 (6.4 - 22.3)	4.8 (3.1 - 8.1)	7.7 (4.8 - 13.4)
Haematological										
	ALB	ALBumin level (plasma)	g/L		23.0 (18.0 - 28.0)	27.0 (23.0 - 32.0)	26.0 (22.0 - 30.0)	24.0 (19.0 - 28.0)	27.0 (23.8 - 31.0)	26.0 (21.0 - 30.0)
	CR	Creatinine level (plasma)	umol/L		210.0 (138.0 - 289.0)	71.0 (58.0 - 91.0)	72.0 (57.0 - 92.0)	72.0 (48.0 - 105.0)	71.0 (56.0 - 87.0)	75.0 (56.0 - 107.0)
	CRP	C-Reactive Protein level (plasma)	mg/L		71.8 (31.0 - 149.0)	56.0 (17.1 - 136.4)	47.0 (12.8 - 104.8)	126.7 (57.8 - 213.7)	63.5 (20.9 - 137.4)	62.5 (25.6 - 138.1)
	POT	POTassium level (plasma)	mmol/L	Continuous	4.3 (3.9 - 5.0)	4.0 (3.6 - 4.4)	4.0 (3.6 - 4.3)	3.9 (3.5 - 4.3)	4.0 (3.6 - 4.3)	4.1 (3.7 - 4.6)
	SOD	SODium level (plasma)	mmol/L		136.0 (133.0 - 140.0)	137.0 (134.0 - 140.0)	137.0 (134.0 - 140.0)	138.0 (135.0 - 142.0)	138.0 (135.0 - 139.0)	138.0 (134.0 - 140.0)
	UR	URea concentration levels	mL		16.1 (10.7 - 23.6)	5.8 (4.2 - 8.3)	5.9 (4.2 - 8.7)	7.3 (4.5 - 11.3)	5.1 (3.7 - 6.8)	6.9 (4.8 - 11.1)

A.14. Descriptive statistics and information of all input data features. Variables are displayed with type, description, units and average statistics. We separate all features according to medical literature, including vital-sign, static, serum and haematological variables. Statistics are shown for each cohort as learnt by our model.